FINITE ELEMENT MODELLING OF UNREINFORCED MASONRY SHEAR WALLETTES STRENGTHENED USING TWISTED STEEL BARS

Robert B. Petersen [a], Najif Ismail [b], Mark J. Masia [a], Jason M. Ingham [b]

[a] Centre for Infrastructure Performance and Reliability, School of Engineering, The University of Newcastle, Callaghan, NSW 2308, Australia
[b] Department of Civil and Environmental Engineering, University of Auckland, Private Bag 92019, Auckland 1142, New Zealand
Author emails: Robert B Petersen robert.petersen@newcastle.edu.au (corresponding author); Najif Ismail nism@auclanduni.ac.nz; Mark J Masia mark.masia@newcastle.edu.au; Jason M Ingham j.ingham@auckland.ac.nz

Abstract

A numerical study was conducted to investigate the in-plane shear behaviour of unreinforced masonry wallettes strengthened with twisted stainless steel reinforcing bars. A two-dimensional finite element model was used to simulate the behaviour of strengthened wallettes tested in diagonal tension in a recent experimental program. The test wallettes included single leaf modern masonry construction and double leaf historical masonry construction. The main aims of the current study were to evaluate the capabilities of the model and to study the behaviour of the wallettes in greater depth. The model was capable of simulating the behaviours of the strengthened wallettes with good accuracy. The model provided insights on the reinforcement mechanism: The reinforcement acts in tension to restrain crack opening, with vertical reinforcement restraining shear-induced crack opening (dilation) to increase the friction along a sliding crack (shear-friction mechanism). The analysis shows that the shear-friction mechanism is significant and requires further investigation. Another finding was that care should be taken when selecting an elastic stiffness for the interface between bar and masonry.

Keywords: masonry; in-plane shear; strengthening; twisted steel bar; finite element.

1. Introduction

In a previous study a finite element (FE) model was designed to simulate the behaviour of masonry wallettes strengthened with near-surface mounted (NSM) fibre-reinforced polymer (FRP) strips [1]. This model was based on a micro-modelling approach and was verified using the results of FRP-strengthened wallettes tested in diagonal tension. These wallettes were single-leaf thick and were strengthened with vertical and/or horizontal FRP strips. In the model the reinforcement was designed to resist sliding via an idealised mechanism, where the reinforcement restrains dilation (crack opening) and increases friction across a sliding joint. The reinforcement also acted in tension to restrain the opening of diagonal cracking through mortar joints and bricks.

In a more recent experimental program, the behaviour of similar masonry wallettes, strengthened this time with NSM twisted stainless steel bars, was investigated [2]. Two different masonry construction types were tested, being single-leaf modern masonry construction (Series 1) and double-leaf historical masonry construction (Series 2). The results of testing reported in Ismail et al. (2011) [2] provided an excellent opportunity to interrogate the capabilities of the FE model developed and verified in Petersen et al. (2010) [1] when considering a different reinforcement type, for historical double-leaf masonry, and when applying different boundary conditions (in the case of Series 2, which will be discussed later).

The observed behaviour of the wallettes as reported in Ismail et al. (2011) [2] was similar to the behaviour of the FRP strengthened wallettes as reported in Petersen et al. (2010) [1]. It was believed that the reinforcing mechanism of the twisted stainless steel bars (in a highly cracked panel) was the same as the mechanism verified for FRP

reinforcement. In this mechanism, the reinforcement acts in tension to restrain dilation, and increases friction along a sliding joint. This mechanism is usually not considered or ignored, but it will be shown in this paper that it is significant. The FE model was developed to reproduce this mechanism.

Work by other researchers on the FE modelling of FRP-strengthened masonry has been reviewed in Petersen et al. (2010) [1]. Other researchers [3-5] have used finite elements to model steel-reinforced masonry. The unique aspect of the model used in Petersen et al. (2010) [1] (and this paper) was the design of the reinforcement connection across sliding cracks (to explicitly model restraint to dilation). Another feature of the model was the treatment of the bond between the masonry and reinforcement using interface elements with debonding behaviour.

The objectives of the research work reported here were to model the wallette tests reported in Ismail et al. (2011) [2] to evaluate the model capabilities, and to study the behaviour of the wallettes in greater detail using the model. In this paper a brief description of the experiments from Ismail et al. (2011) [2] is provided first. The FE models are then described, and the material property sets used in the models are presented. The results of the FE model simulations are then compared to the experimental results. Comments about the accuracy of the model and recommendations for future work are then provided.

2. Experimental Program

A brief description of the tested wallettes from Ismail et al. (2011) [2] is provided in this section. The test wallettes were constructed and tested in two series: Series 1

(single-leaf modern masonry construction) and Series 2 (two-leaf historical masonry construction). The wallettes in both series were tested in diagonal tension/shear in accordance with ASTM E519-02 [6]. Test wallettes were given the notation WXC-N or WXS-N, where W refers to wallette, X denotes the test series (1 or 2), C refers to unreinforced control specimens, S refers to strengthened reinforced specimens and N denotes the test number.

Series 1 involved testing two URM and eight strengthened wallettes. Series 1 wallettes were approximately 1200 mm x 1200 mm, and were constructed from a single leaf of solid extruded clay bricks and 10 mm mortar joints (Figure 1). New bricks with nominal dimensions of 230 mm long x 110 mm wide x 76 mm high were used. The mortar was mixed in several batches, with mix proportions of 1:1:6 (cement: lime: sand by volume) plus an air entraining admixture.

Series 2 involved testing one URM and six strengthened wallettes, with each wallette being approximately 1200 mm x 1200 mm in size and double-leaf thick. Series 2 wallettes were constructed using salvaged solid clay bricks laid in a common bond pattern (i.e. one header course after every three stretcher courses), with roughly 15 mm thick mortar joints (Figure 1). Salvaged bricks with approximate dimensions of 220 mm long x 105 mm wide x 90 mm high were used. The mortar was mixed in several batches, with mix proportions of 1:2:9 (cement: lime: sand by volume).

The average properties of the materials used to construct the test wallettes (both series) are shown in Table 1. These properties were determined from material characterisation tests performed alongside the wallette construction and testing programs.

Bond wrench tests, used to determine the flexural tensile bond strength (f_{mt}) of the masonry, were performed on each mortar batch used in the construction of Series 1 wallettes (in accordance with AS3700:2001 [7]). Table 2 shows the f_{mt} values for the batches used to construct these wallettes. These bond strength values were used to estimate different mortar joint material property sets for the FE modelling (Section 3.4). Separate material data results for each wallette in Series 2 were not available.

The wallettes in both test series were strengthened using the same type of high-strength twisted stainless-steel reinforcing bars. Two different sized bars were used: 6 mm outside diameter (Series 1&2), and 10 mm outside diameter (Series 1 only). The reinforcing bars were bonded, using an injectable cementitious grout, into rectangular slots cut into the surface of the masonry (near-surface mounting technique). A 30 mm deep x 10 mm wide slot was cut for the 6 mm diameter bars, and a 30 mm deep x 14 mm wide slot was cut for the 10 mm diameter bars. In most cases only a single bar was placed in each slot. However, in the case of wallettes W1S-3 and W1S-4, two 6 mm bars were inserted into each slot, and for wallettes W1S-5 and W1S-6, two 10 mm bars were inserted into each slot. The material and geometrical properties of the bars are shown in Table 1.

The locations and details of the reinforcing bars are shown in Figure 2. The vertical slots were either located in the brick units, midway between mortar head joints, or through alternating brick units and mortar head joints. All of the horizontal slots were located in the mortar bed joints. Strengthening was applied to both faces of the Series 1 wallettes, whereas for Series 2 wallettes strengthening was only applied to one side of the wallette.

The test setup was different for each test series. Series 1 wallettes were tested under the standard test conditions outlined in ASTM E519-02 [6]. Series 2 wallettes were tested using a modified test setup because the wallettes were heavy and had low bond strength. Note that Series 2 wallettes were constructed directly on top of steel beams with no mortar between the wall and steel beam. Figures of the test setup are shown in Figure 3.

3. Finite Element Modelling

3.1 Modelling Approach

The FE modelling approach is discussed in this section. More information on the model development strategy can be found elsewhere [1]. The commercial FE analysis package DIANA 9 [8], which is based on the displacement finite element method, was used for this study. All of the wallettes were modelled in two dimensions (in the plane of the wallette). Therefore out-of-plane effects, possibly affecting the in-plane behaviour of wallettes with single-sided strengthening (Series 2), were not accounted for.

The multi-surface interface model of Lourenço and Rots (1997) [9] was used to model the masonry. The brick units were modelled with elastic continuum elements, and the mortar joint and unit/mortar interface were lumped into interface elements (with zero thickness). Potential mid-brick cracking was also modelled using interface elements. As the mortar joint was modelled with zero thickness, the brick units were expanded to maintain the wallette geometry.

The brick units were modelled using eight-node, quadratic, rectangular, plane-stress elements. The interface elements (mortar joint and mid-brick crack) were modelled using six-node, quadratic, rectangular, plane-stress interface elements. An example of the mesh, with mesh divisions, is shown in Figure 4 (single leaf masonry).

Non-linear behaviour in the mortar joint interface elements was modelled using the Crack-Shear-Crush material model in DIANA 9. The model is based on multi-surface plasticity and includes: a Coulomb friction model (to simulate shear-cracking and shear-friction); a tension cut-off model (to simulate tension cracking); and an elliptical compression cap model (to simulate shear-compression). The model also includes crack opening due to sliding (dilation).

Non-linear behaviour in the potential brick crack interface elements was modelled using a linear tension softening model. These interface elements were modelled as initially very stiff, with zero shear stiffness after tensile cracking.

The twisted steel bars, and their connection to the masonry, were modelled using the same approach used to model the FRP strips as reported in Petersen et al. (2010) [1] (see Figure 4). The bars were modelled using two-node linear truss elements, and were connected to the masonry using zero-thickness interface elements (six-node, quadratic, rectangular, plane-stress), representing the grout. Yield was incorporated into the bars using a Von Mises failure model.

To connect the bar truss elements across mortar joint and brick crack interface elements a zero-thickness node interface element was used (Figure 4). This element was given a high stiffness in the bar's longitudinal direction to make the bar continuous across

joints, and was given a low stiffness in the transverse direction to ignore bar dowel capacity.

Figure 4 also shows where the bars were connected (via interface elements) to the brick units for each different bar location adopted in the experiments. The bars being located in the following slots: (i) vertical slots cut into brick units, midway between mortar head joints, (ii) vertical slots cut through alternating brick units and head joints, and (iii) horizontal slots cut into the mortar bed joints. Note that the horizontal bar elements were only attached to bricks on one side of the mortar bed joint for simplicity. Similarly, the vertical bar elements (case ii) were only attached to bricks on one side of the head joints. As a result, any extra shear strength that the grout provided to the bed/head joints in the experiments was not accounted for in the models. One model was generated with the vertical bar elements attached to the bricks on both sides of the reinforcement, to investigate the effect of the extra shear strength. The extra shear strength provided by the grout to the head joints was found to be insignificant.

3.2 Series 1 Wallette Models

An example Series 1 wallette model is shown in Figure 5a. A fixed support was modelled at the location of the bottom loading shoe, and a stiff steel section was used to simulate the top loading shoe. The stiff steel section was modelled with the same element type as the brick units. At the top of the steel section a roller support was used to restrain movement in the x-direction.

A self-weight of 2.09 kN/m^2 was assumed for the 110 mm thick masonry (AS/NZS 1170.1:2002 Table A2) [10]. This self-weight was applied as a downwards vertical pressure load on the brick units in the models.

The vertical compression load at the top corner of the wall was simulated by applying a vertical displacement, incremented in 0.01 mm steps (displacement control). A linear iteration scheme was used to solve for equilibrium at each displacement increment.

3.3 Series 2 Wallette Models

An example Series 2 wallette model is shown in Figure 5b. Series 2 wallettes were modelled in two layers, one layer for the front leaf and one layer for the back leaf. The two layers were connected to: common header units at every fourth course, and stiff steel sections representing the loading shoes in the corners. The stretcher units of each leaf, above and below the common header units, were connected to the header units with mortar joint interface elements. The leaves were connected to the loading shoes using stiff elastic interface elements. In the 2D model the nodes of both layers/leaves were located in the same position in space, but both layers were distinct (except the common header unit). The vertical reinforcement was attached (via interface elements) to the stretcher units on the back leaf, as well as the common header units. The horizontal reinforcement was attached (via interface elements) to the top of the header units.

Interface elements were attached to the base the wall (both leaves) to model the frictional contact between the wall base and base beam. The nodes at the bottom of these interface elements were restrained against translation to simulate the base beam restraint.

To model self-weight, downwards vertical pressures of 1.94 kN/m^2 and 3.89 kN/m^2 were applied to the stretcher and header units, respectively. These pressures were based on a brick density of 1800 kg/m^3.

Two diagonal compressive loads (P) (oriented in-line with the wallette diagonal) were applied to the wallette model to simulate the compressive loading on the wallette. To capture the non-linear load displacement of the wallette, arc-length control was adopted. The loads were applied in steps of 1.414 kN, and arc-length control was applied to the node in the top-right corner of the wallette in the negative x-direction.

3.4 Series 1 Geometrical and Material Properties

The geometrical properties are the thickness of the plane stress elements and the area of the truss elements. A plane stress thickness of 110 mm (wallette thickness) was adopted for the brick unit elements, the mortar joint interface elements, the mid-brick interface elements, and the stiff steel section elements (loading shoe). Only a single bar was created in the model at each slot location, even for cases where two bars were located in each slot (in the experiments). To account for the additional bar in the slot, the area of the reinforcing bar truss elements was simply doubled. The bar element areas used were: 7.14 mm^2 for one 6mm diameter bar/slot; 14.28 mm^2 for two 6mm diameter bars/slot; and 29.6 mm^2 for two 10mm diameter bars/slot.

The plane stress thickness of the grout interface elements (connecting the bars to the masonry) was taken as the bonded perimeter along the grout-masonry interface. The bonded perimeter of the 30 mm x 10 mm slots was equal to 70 mm, and the bonded perimeter of the 30 x 14 mm slots was equal to 74 mm.

The material properties used in the FE analyses (Series 1) were based on the material properties determined at the time of testing (Tables 1 and 2), material characterisation tests conducted as part of a previous investigation [1], and also recommendations from the literature.

For the brick unit elements an elastic modulus of 27,600 MPa was adopted; a Poisson's ratio of 0.2 was assumed based on recommendations in Lourenço (1996) [11]. The brick elastic modulus was determined from compression tests on masonry prisms [12]. For the mid-brick crack interface elements a direct tensile strength of 2.4 MPa was adopted. This value was estimated as the flexural tensile strength of the brick (3.6 MPa, Table 1) divided by 1.5 (reasons for this reduction are given in Petersen (2009) [12]). The tensile fracture energy was assumed as 0.025 N/mm based on recommendations from Lourenço (1996) [11].

The different bond strength values for each different wallette of Series 1 (Table 2) were used to estimate different mortar joint material property sets for the FE modelling, as mentioned before. The bond strength values of wallettes W1C-1 & W1C-2, W1S-1 & W1S-2, and W1S-3 & W1S-4 were all similar, and therefore the same mortar joint material property set was used for these wallettes. The mortar joint material data sets adopted for the Series 1 wallettes are shown in Table 3.

The properties in Table 3 were estimated using the results of material characterisation tests conducted in a previous investigation [1]. These material characterisation tests produced two data sets; one for mortar joints with a high flexural tensile bond strength (f_{mt} = 1.22 & 1.74 MPa), and one for mortar joints with a low flexural tensile bond strength (f_{mt} = 0.176 & 0.14 MPa). The material properties for each

wallette were estimated using linear interpolation between the two experimentally determined data sets, based on the wallette bond strength.

The initial run of the control wallette FE model (to model wallettes W1C-1 & W1C-2) gave an ultimate load of 126 kN. This value was less than the average ultimate loads of the two experiments (W1C-1 & W1C-2), which was 143 kN. The cohesion value was adjusted in the control wallette data set (column 2 of Table 3), from 0.37 to 0.5 MPa, so that the model also gave an ultimate load of 143 kN. This adjusted cohesion was then used in the other models sharing the same data set as the control wallettes (column 2, Table 3).

For the stainless steel bars, the manufacturers quote a range for the elastic modulus of the bars between 110 and 180 GPa (Table 1). For the models a mid-range value of 145 GPa was adopted. Models were also tested using the extreme values of the elastic modulus (110 and 180 GPa). The difference in bar elastic modulus values did change the load-displacement behaviour of the model wallettes, but the change in results fit within the variability observed in the experimental tests. A Poisson's ratio of 0.3 was assumed. The yield stress of the bars was assumed equal to the 0.2 % proof stress: 913 MPa for the 6mm diameter bar and 892 MPa for the 10mm diameter bar.

The 'grout' elements represented the connection (bond) of the bars to the masonry, with the elements loaded in the shear direction with bar tension. These elements were assumed to behave elastically, with no debonding. This assumption was based on the following findings: (i) debonding (of the bars from the masonry) was not observed in any wallette tests whereas bar rupture was observed in some cases; (ii) in pull-out tests

the peak tensile force in the bars was close to the nominal bar tensile strength and no debonding was observed [2].

The shear stiffness of the bond between the bar and masonry was not experimentally determined, hence this value needed to be assumed for this analysis. A shear stiffness of 60 N/mm^3 was estimated as a starting value, based on the bond shear stiffness between a carbon FRP strip and masonry [1]. The sensitivity of the model to this parameter was also assessed by running models with the following bond shear stiffness values: 10, 1000, 10000 N/mm^3 (very stiff).

3.5 Series 2 Geometrical and Material Properties

A plane stress thickness of 110 mm (half-wallette thickness) was adopted for the stretcher unit elements and the following interface elements: mortar bed joint, mortar head joint (between stretcher units), mid-brick, those between the wall base and base beam, and those between the masonry leaves and the loading shoes. A plane stress thickness of 220 mm (wallette thickness) was adopted for the header unit elements, the stiff steel section elements (loading shoe), and the mortar head joint interface elements (between header units). The geometrical properties of the bar (one 6mm diameter bar/slot) and grout elements were the same as in Series 1.

For the brick unit elements an elastic modulus of 6,000 MPa was assumed (based on data for a similar brick with a similar compressive strength [13]). A Poisson's ratio of 0.2 was assumed (based on recommendations in Lourenço (1996) [11]). For the mid-brick crack interface elements a direct tensile strength of 2.6 MPa was adopted. This value was estimated as the flexural tensile strength of the brick (Table 1) divided by 1.5.

The tensile fracture energy was assumed as 0.075 N/mm based on recommendations from Lourenço (2008) [14].

Only a single mortar joint material data set was used for Series 2 wallettes, as separate material data results for each wallette in Series 2 were not available. The material properties used in the models are summarised in Table 4. Most properties were estimated based on the recommendations given in a draft document written by the New Zealand Society for Earthquake Engineering [15]. The cohesion was increased from 0.06 to 0.08 MPa, so that the ultimate load given in the control wallette model was the same as the ultimate load of wallette W2C-3.

The material properties of the 6mm diameter bars used in the Series 2 wallettes were the same as those used in the Series 1 wallettes. For the grout interface elements an interface shear stiffness of 60 N/mm^3 (the same as Series 1 wallettes) was adopted.

4. Results

4.1 Series 1 Wallette Models

The load-displacement curves and crack patterns predicted by the models closely matched those recorded and observed in the experiments. The load-displacement curves of the tested wallettes and the FE models are shown in Figure 6. For the load-displacement curves the displacement is defined as the vertical displacement of the top loading shoe in the model as shown in Figure 5a. In the experiments the vertical displacement was measured using a potentiometer across a gauge length of 1414 mm. Note that the displacement measured across a gauge length of 1414 mm in the model was approximately the same as the displacement of the top loading shoe. The crack patterns

of some selected models are shown with photographs of the tested wallettes in Figure 8. In the case of the unreinforced control wallette, both the experimental wallettes and the FE model failed by a single diagonal crack through the mortar joints (Figures 8a and 8d). In the vertically reinforced wallettes (FE models and experiments), failure along a single diagonal crack was prevented, and instead many diagonal cracks developed (Figures 8c and 8f). For the horizontally reinforced wallettes, failure occurred by sliding along a crack through an unstrengthened bed joint at the top of the wallette (Figures 8b and 8e). In both the experiment and FE model this failure mode only occurred after a diagonal crack formed but was restrained by the reinforcement.

The FE models provided an opportunity to study the tensile stresses in the reinforcing bars, which is a property that could not be measured during the tests. Stresses in the bars could not be measured reliably using strain gauges because of the helical profile of the bar. Some example bar tensile stress distributions are illustrated on the bars themselves in Figures 8e and 8f. The maximum bar tensile stresses for the wallettes were: W1S1&2 – 913 MPa (yield at 9.2 mm wallette displacement); W1S3&4 – 840 MPa (at 12 mm); W1S5&6 – 694 MPa (at 12 mm); and W1S7&8 – 525 MPa (at 3 mm). Note that yielding of the bars occurred in the W1S1&2 model. This result is consistent with what happened in the W1S-1 and W1S-2 experiments, where bar yielding followed by bar rupture occurred.

As mentioned before in Section 3.4, a sensitivity study on the elastic shear stiffness of the grout interface element (k_{bs}) was performed. Load-displacement curves of the W1S-1&2 model with different k_{bs} values, ranging from 10 to 10000 N/mm^3, are shown in Figure 9. Very high k_{bs} values represent a ‘perfect bond’, and when used in this

model, greatly overestimate the load. Care should therefore be taken when selecting an elastic stiffness for the interface between the bar and the masonry.

4.2 Series 2 Wallette Models

The FE model displayed good agreement for the Series 2 unreinforced wallette, in terms of both the crack pattern (Figures 10a and 10d) and the shape of the load-displacement curve (Figure 7a). The displacement was measured, in-line with the applied load, across a gauge length of 1414 mm (model and experiment). In both the model and experiment, cracks developed in the mortar joints along the compressed diagonal.

The FE models produced reasonable approximations of the Series 2 strengthened wallettes, given that the material properties were assumed and the wallette variability was unknown (no test repeats). The load-displacement curves of the Series 2 strengthened wallettes (model and experiment) are shown in Figure 7. In general the model did not capture the initial peak load, but the residual capacity was well-captured. The differences between the experiment and model simulation could be attributed to the following factors: differences between the assumed material properties for the model and the largely unknown properties of the real material, the unknown variability of the test wallettes, the difference between the experiments and the “perfect” model, and that the model was unable to capture the three-dimensional effects of the wallette which was strengthened on one side only.

The crack patterns/failure modes of the FE models (strengthened wallettes) were consistent with those observed in the experiments. The crack patterns of some selected models are shown with photographs of the tested wallettes in Figure 10. In the case of the

horizontally strengthened wallette (W2S-14), the experiment failed by diagonal cracking in the mortar joints as shown in Figure 10b. The FE model failed in a combination of diagonal cracking through the mortar joints, and sliding along near-horizontal bed joint cracks (Figure 10e). For the vertically strengthened wallettes (FE model and experiments), the reinforcement allowed many diagonal cracks to develop in the mortar joints. The crack pattern of wallette W2S-11 is shown in Figures 10c and 10f. The other strengthened wallettes displayed similar crack patterns (FE models and experiments). Bar yield occurred in all models except for W2S-14. Bar rupture was not observed in the experiments, but bar yielding may have occurred.

5. Conclusions

A finite element model was used to simulate the in-plane shear behaviour of unreinforced masonry wallettes strengthened with twisted stainless steel bars, which were tested in a previous study [2]. The test wallettes were constructed and tested in two series: Series 1 (single-leaf modern masonry construction) and Series 2 (two-leaf historical masonry construction). Series 1 consisted of two URM wallettes and eight strengthened wallettes, and Series 2 consisted of one URM wallette and six strengthened wallettes. Finite element models were made for each wallette.

The following conclusions were drawn from the study:

- The model, previously verified for FRP-strengthened masonry tested in shear, is capable of simulating the in-plane shear behaviour of unreinforced masonry strengthened with the different reinforcing material – the twisted steel bars;

- The two-dimensional model is capable of simulating the behaviour of unreinforced double-leaf historical masonry construction and provides a good approximation of the behaviour of double-leaf historical masonry strengthened with twisted steel bars;
- The main reinforcing mechanism of vertical twisted steel reinforcing bars is the same mechanism as determined for FRP – the reinforcement acts in tension to restrain crack opening (dilation), increasing friction along a sliding crack. This conclusion was confirmed because the model, which is based on the mechanism described, generated output that closely matched the experimental results of the Series 1 strengthened wallettes.
- The analysis in this paper shows that the shear-friction mechanism of vertical reinforcement is significant. Thus the work in this paper is valuable in that it highlights the need for further investigation of the mechanism.
- Care should be taken when selecting an elastic stiffness for the interface between bar and masonry. Using a 'perfect' bond may lead to large errors in wall behaviour and ultimate load.

6. Acknowledgements

Financial support for this project was provided by the Australian Research Council under Discovery Project DP 0879592 and by the New Zealand Foundation for Research, Science and Technology under grant UOAX0411. The Higher Education Commission of Pakistan provided funding for the doctoral studies of Najif Ismail.

7. References

[1] Petersen RB, Masia MJ, Seracino R. In-plane shear behavior of masonry panels strengthened with NSM FRP strips. II: Finite Element Model. Journal of Composites for Construction 2010; 14(6): 764-774.

[2] Ismail N, Petersen RB, Masia MJ, Ingham JM. Diagonal shear behaviour of unreinforced masonry wallettes strengthened using twisted steel bars. Constr Build Mater 2011; 25(12): 4386-4396.

[3] Mittal AK. Nonlinear finite element analysis of reinforced hollow concrete block masonry wall. Individual Studies by Participants at the International Institute of Seismology and Earthquake Engineering 1999; 35: 229-241.

[4] Ewing RD, Kariotis JC, El-Mustapha A. Nonlinear finite element analysis of experiments on two-storey reinforced masonry shear walls. Struct Des, Anal Test 1989*;* 979-988.

[5] Dhanasekar M., Haider W. Explicit finite element analysis of lightly reinforced masonry shear walls. Computers and Structures 2008; 86(1-2): 15-26.

[6] ASTM Committee E-519-02. Standard test method for diagonal tension (shear) in masonry assemblages. American Society for Testing and Materials International, 2002.

[7] AS Committee 3700. Masonry Structures: Appendix D – Method of test for flexural strength. Standards Australia, 2001.

[8] TNO DIANA. DIANA 9 users manual. D. Tno, ed., Delft, The Netherlands, 2005.

[9] Lourenço PB, Rots JG. A multi-surface interface model for the analysis of masonry structures. Journal of Structural Engineering 1997; 123(7): 660-668.

[10] AS/NZS Committee 1170.1. Structural design actions – Permanent, imposed and other actions. Standards Australia, 2002.

[11] Lourenço PB. A user/programmer guide for the micromodeling of masonry structures. *TU-DELFT Rep. No. 03.21.1.31.35*, Delft Univ. of Technology, Delft, The Netherlands, 1996.

[12] Petersen RB. In-plane shear behaviour of unreinforced masonry panels strengthened with fibre reinforced polymer strips. Ph.D. thesis, School of Engineering, The Univ. of Newcastle, Newcastle, New South Wales, 2009.

[13] Rots JG. Structural masonry: an experimental/numerical basis for practical design rules. Rotterdam: Balkema; 1997.

[14] Lourenço PB. Structural masonry analysis: Recent developments and prospects. In: Masia M, Totoev Y, Page A, Sugo H, editors. 14th International Brick and Block Masonry Conference, Sydney, Australia: The University of Newcastle; 2008. Keynote paper.

[15] Ingham J, editor. Assessment and Improvement of Unreinforced Masonry Buildings for Earthquake Resistance, Wellington, New Zealand: New Zealand Society for Earthquake Engineering; 2011.

[16] Van der Pluijm, R. (1997). Non-linear behaviour of masonry under tension. Heron 1997; 42(1): 25-54.

[17] Van Zijl GPAG. Modeling masonry shear-compression: Role of dilatancy highlighted. J. Eng. Mech. 2004; 130(11): 1289-1296.

Table 1. Material properties from Ismail et al. (2011) [2]

Masonry Materials						
Series		**f'_b MPa**	**f_{bt} MPa**	**f'_j MPa**	**f_c MPa**	**f_{mt} MPa**
1	Value	-	3.6	-	32.1	0.4
	COV	-	21%	-	18%	37%
2	Value	39.4	3.9	1.4	10.7	0.2
	COV	48%	14%	30%	33%	29%
Reinforcing Steel						
	D mm	**f_{py} MPa**	**f_{pu} MPa**	**f_{ps} MPa**	**E_{ps} $\times 10^3$ MPa**	**A_s mm^2**
1,2	6	913	1168	697	110-180	7.14
	10	892	1108	470		14.8

Where: f'_b = brick compressive strength; f_{bt} = brick modulus of rupture; f'_j = mortar compressive strength; f_c = masonry compressive strength; f_{mt} = flexural tensile strength of masonry; f_{py} = specified 0.2% proof stress of reinforcement; f_{pu} = specified ultimate tensile strength of reinforcement; f_{ps} = shear strength of reinforcement; E_{ps} = elastic modulus of reinforcement; D = outer bar diameter; and A_s = net cross sectional bar area.

Table 2. Series 1 Wallette Flexural Tensile Bond Strength (f_{mt}) Data

Wallette	Masonry average f_{mt} (MPa) (COV%)
W1C-1 & W1C-2	0.41 (36)
W1S-1 & W1S-2	0.44 (45)
W1S-3 & W1S-4	0.44 (43)
W1S-5 & W1S-6	0.59 (30)
W1S-7 & W1S-8	0.21 (29)

Table 3. Material properties adopted for mortar joint interface elements (Series 1)

Property	**Wallette**		
	W1C-1 & W1C-2 W1S-1 & W1S-2 W1S-3 & W1S-4 (f_{mt} = 0.44 MPa)	W1S-5 & W1S-6 (f_{mt} = 0.59 MPa)	W1S-7 & W1S-8 (f_{mt} = 0.21 MPa)
Normal stiffness k_n (N/mm^3)	388	433	318
Shear stiffness k_s (N/mm^3)	161	180	132
Tensile strength f_t (MPa)	0.29	0.39	0.14
Tensile fracture energy G^I_f (N/mm)	0.007	0.007	0.005
Cohesion c_0 (MPa)	0.37 (0.5)[a]	0.44	0.25
Friction coefficient (initial) Φ_i	0.90	0.90	0.90
Friction coefficient (residual) Φ_r	0.62	0.66	0.57
Dilation coefficient (initial) Ψ_0	0.54	0.56	0.51
Confining normal stress to cause zero dilation σ_u (MPa)	-0.9	-1.0	-0.8
Dilation degradation coeff. δ	1.9	1.9	1.8
Compressive strength f_c (MPa)	23	25	20
Comp. fracture energy G_c (N/mm)	23	23	22
Plastic strain at f_c, κ_p	0.014	0.016	0.010
Shear fracture energy G^{II}_f (N/mm)	$0.035\text{-}0.49\sigma_n$	$0.035\text{-}0.49\sigma_n$	$0.035\text{-}0.49\sigma_n$

[a] - Cohesion calibrated to match average ultimate load of URM wallettes W1C-1 and W1C-2.

Table 4. Material properties adopted for mortar joint interface elements (Series 2)

Property	Value	Source/notes
k_n (N/mm^3)	66	Determined using equations given in Lourenço (1996) [11], based on material properties: elastic modulus masonry = 3210 MPa [15] (f_c = 10.7 MPa), elastic modulus brick = 6000 MPa (assumed, see Section 3.5), Poisson's ratio of brick and mortar = 0.2 (assumed, [11])
k_s (N/mm^3)	28	
f_t (MPa)	0.02	Assumed equal to f_{mt} /1.5. [16]. f_{mt} = 0.035 MPa [15] (f'_j = 1.4 MPa).
G^I_f (N/mm)	0.005	Assumed. G^I_f for a masonry joint with low tensile strength f_t = 0.1 MPa [17].
c_0 (MPa)	0.06 (0.08)[a]	Initial value 0.06 MPa [15] (f'_j = 1.4 MPa). Calibrated value 0.08, refer to text.
Φ_i	0.65	Recommended [15]
Φ_r	0.65	Recommended [15]
Ψ_0	0.5	Assumed. Properties determined from experimental torsion shear tests, on masonry similar to Series 2, with f_{mt} = 0.14 MPa [1].
σ_u (MPa)	-0.75	
δ	1.8	
f_c (MPa)	10.7	Table 1
G_c (N/mm)	17.12	Determined using equations given in Lourenço (2008) [14], using f_c
κ_p (mm)	0.001	Assumed. [11]
G^{II}_f (N/mm)	0.02-0.17σ_n	Assumed. Lower bound, precompression-dependent, relationship from torsion shear tests on masonry similar to Series 2 [1].

[a] - Cohesion calibrated to match ultimate load of URM wallette W2C-3.

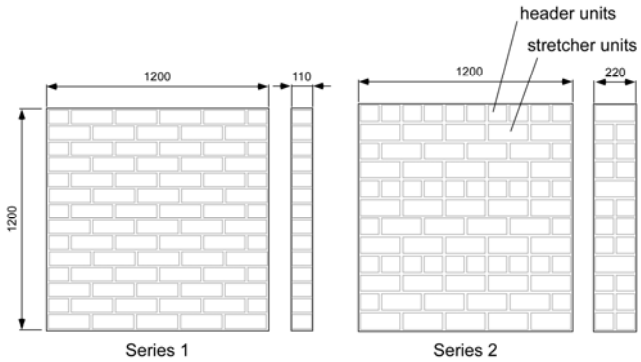

Figure 1. Wallette Bond Patterns from Ismail et al. (2011) [2]

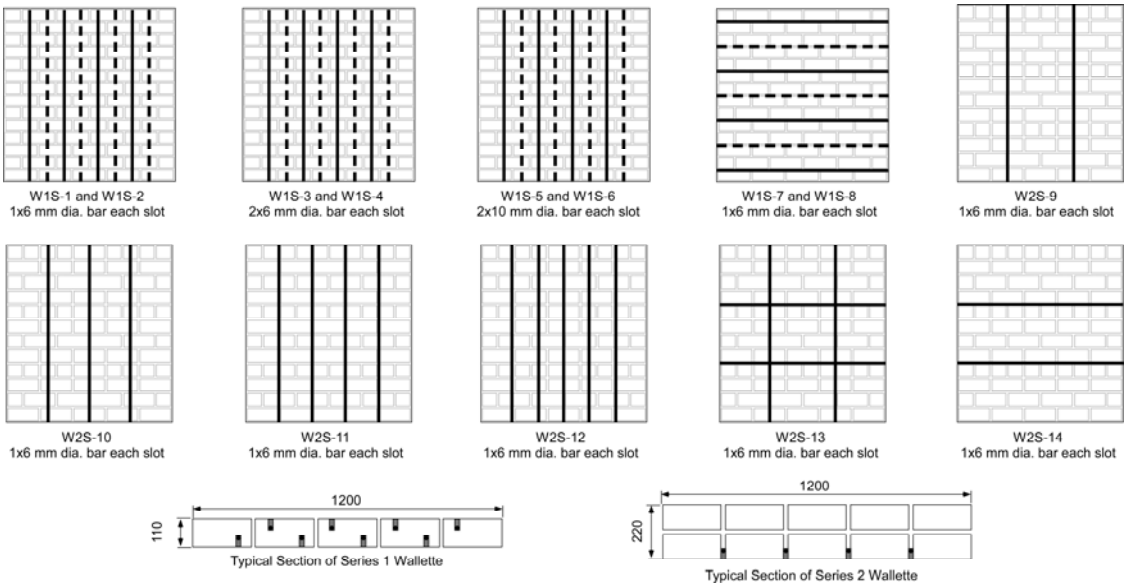

Figure 2. Strengthened wallette details from Ismail et al. (2011) [2]
(Dashed lines represent bars installed on rear face – Series 1)

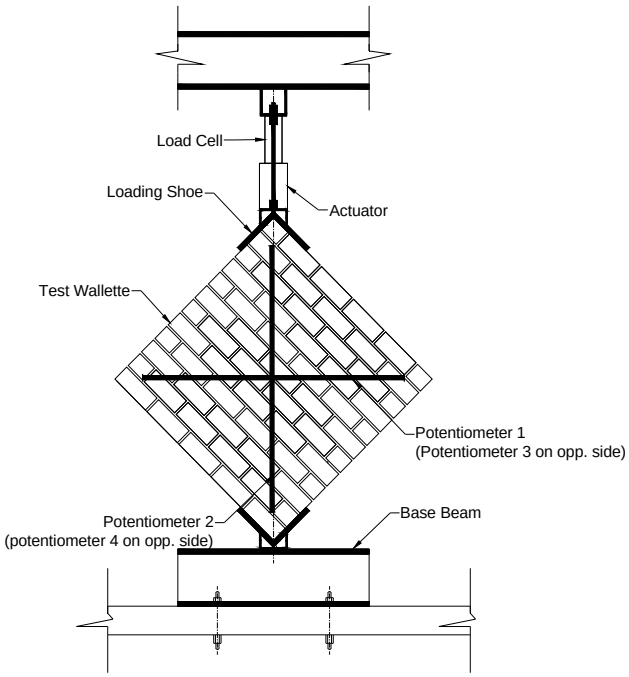

(a) Standard test setup (Series-1)

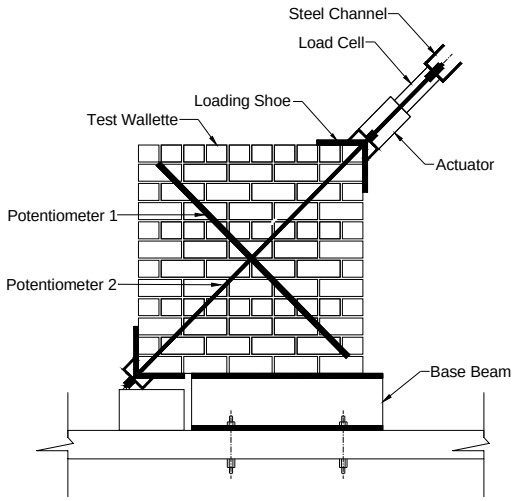

(b) Modified test setup (Series-2)

Figure 3. Test Setups from Ismail et al. (2011) [2]

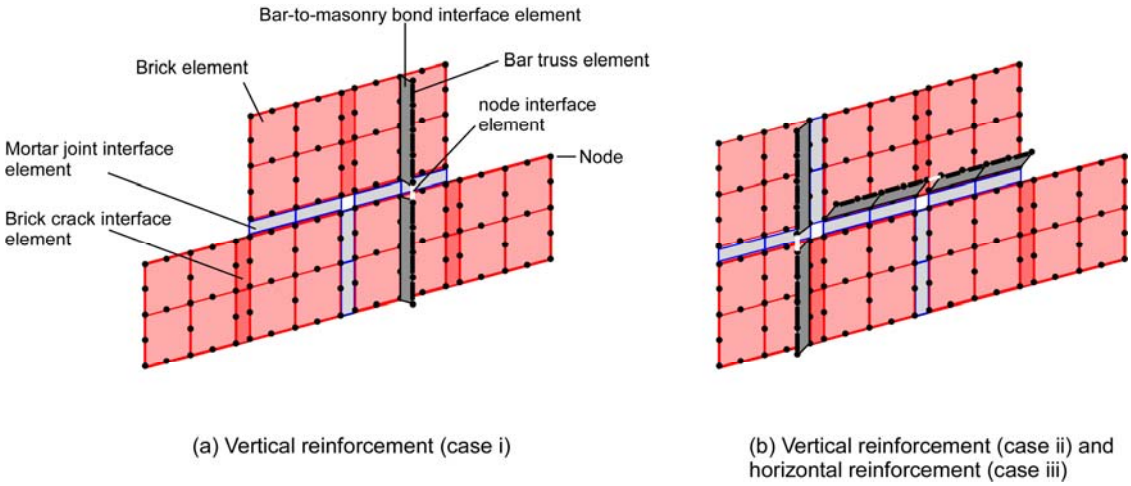

Figure 4. Masonry FE mesh, with twisted steel bar attachment

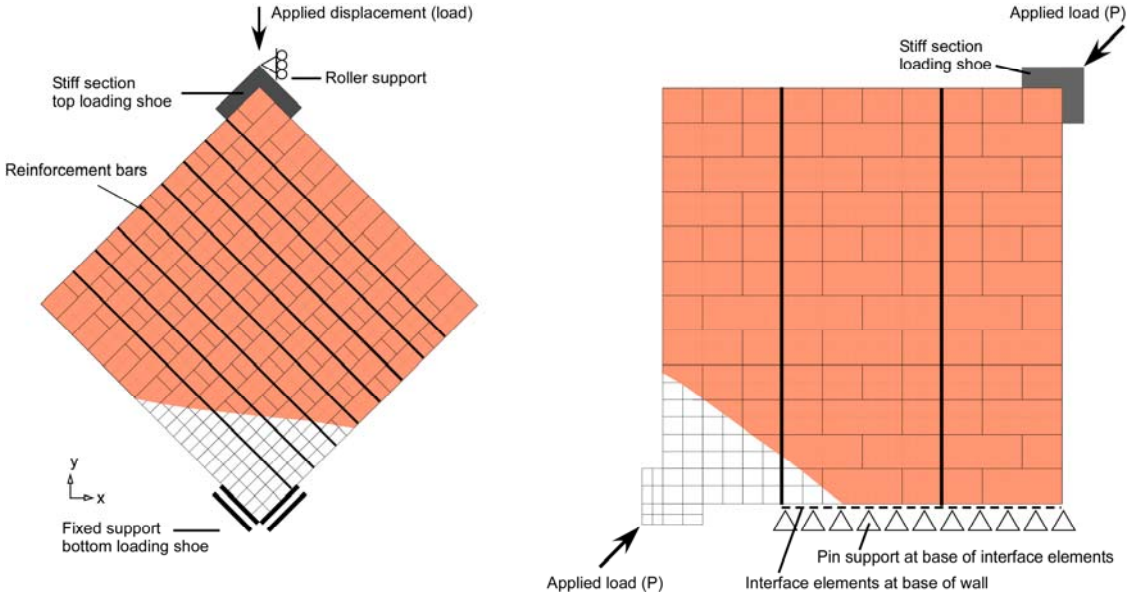

(a) Series 1 (W1S-1 and W1S-2) (b) Series 2 (W2S-9)

Figure 5. Wallette models (mesh shown in bottom corners)

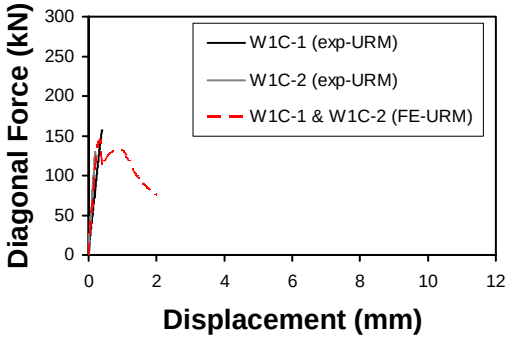

(a) W1C-1 and W1C-2 (URM wallettes)

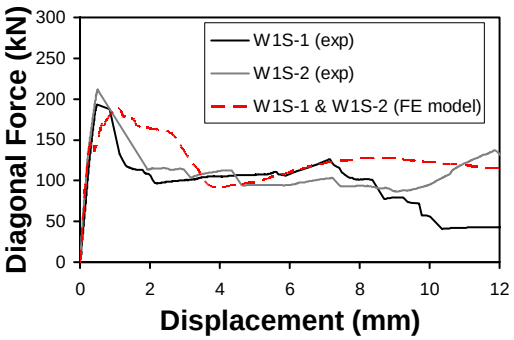

(b) W1S-1 and W1S-2

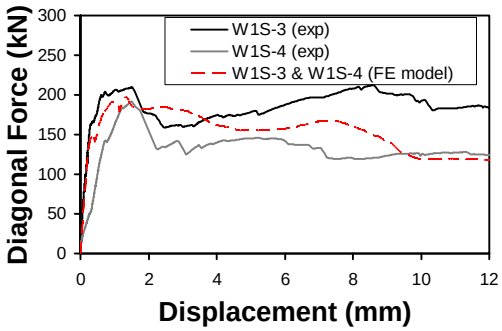

(c) W1S-3 and W1S-4

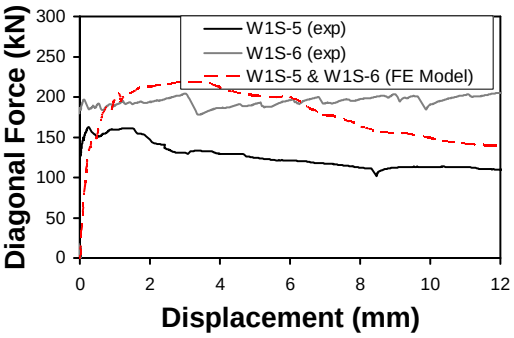

(d) W1S-5 and W1S-6

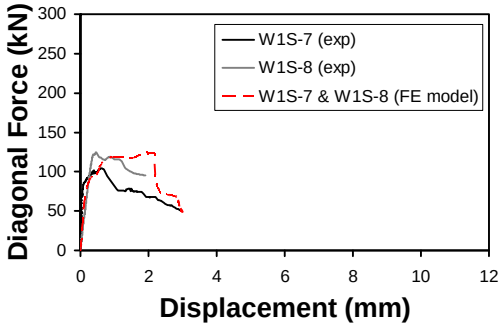

(e) W1S-7 and W1S-8

Figure 6. Load-displacement plots Series 1 Wallettes. Experimental results shown with unbroken lines, FE model results shown with broken lines

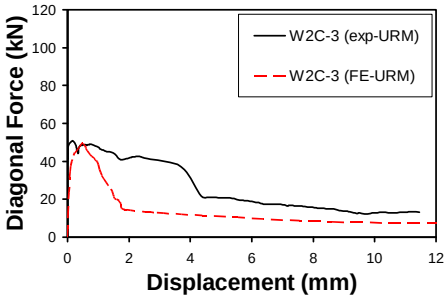

(a) W2C-3

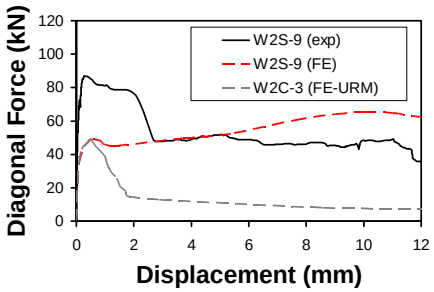

(b) W2S-9

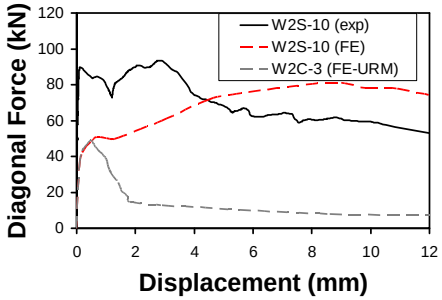

(c) W2S-10

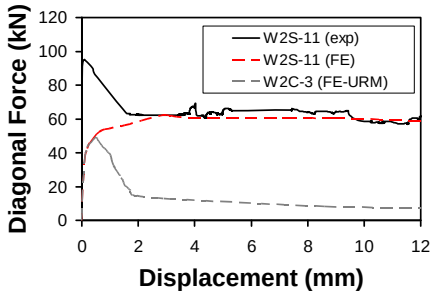

(d) W2S-11

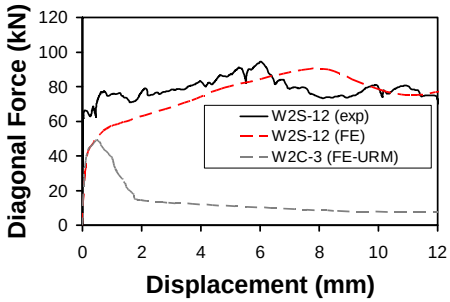

(e) W2S-12

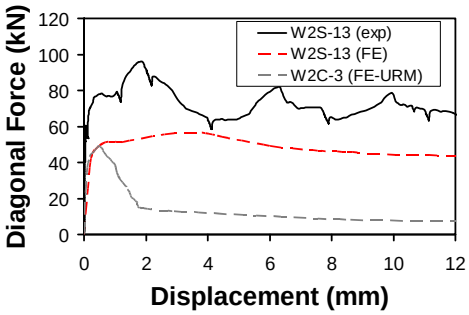

(f) WS2-13

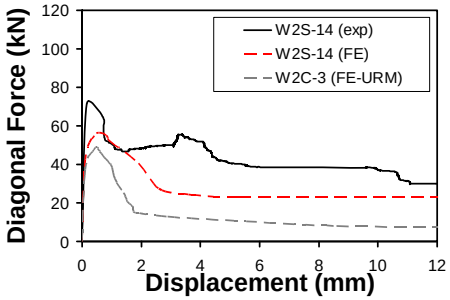

(g) WS2-14

Figure 7. Load-displacement plots Series 2 Wallettes. Experimental results shown with unbroken lines, FE model results shown with broken lines

(a) Unreinforced control wallette W1C-1

(b) Horizontally reinforced wallette W1S-7

(c) Vertically reinforced wallette W1S-5

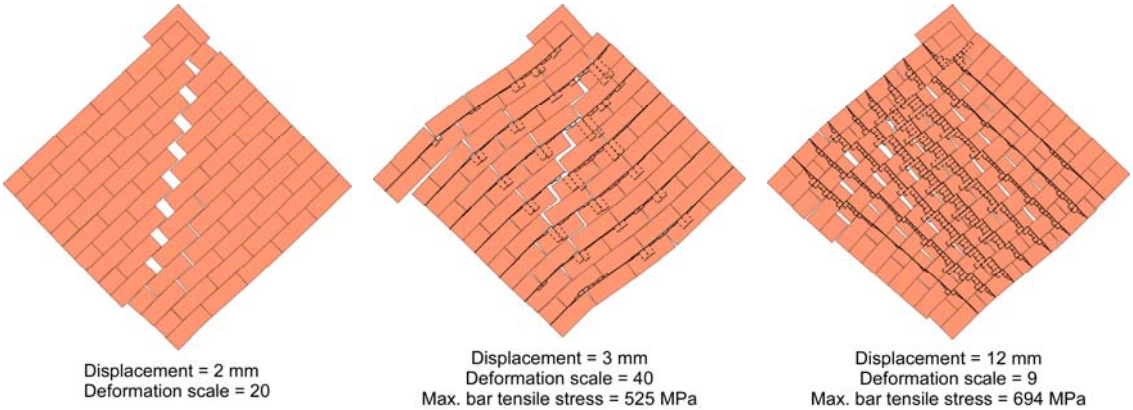

(d) FE model W1C-1&2

(e) FE model W1S-7&8

(f) FE model W1S-5&6

Figure 8. Series 1 wallette crack patterns

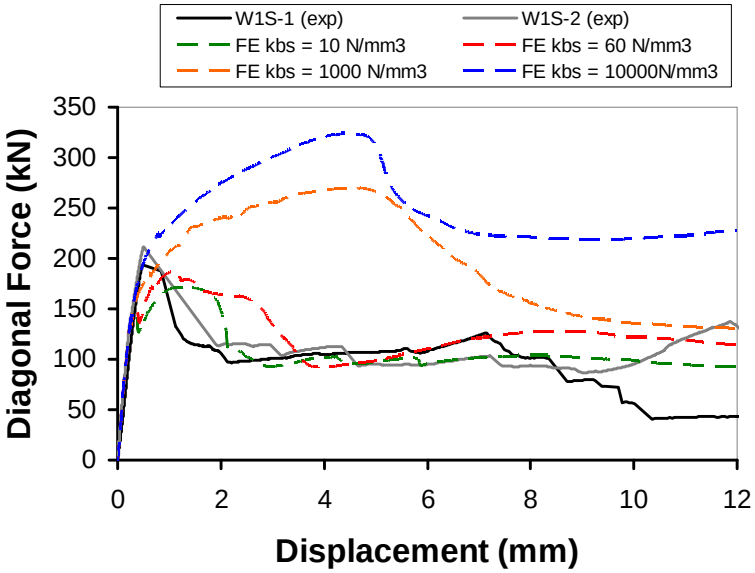

Figure 9. Sensitivity study on the elastic shear stiffness of grout interface element (k_{bs}) (W1S-1&2 model)

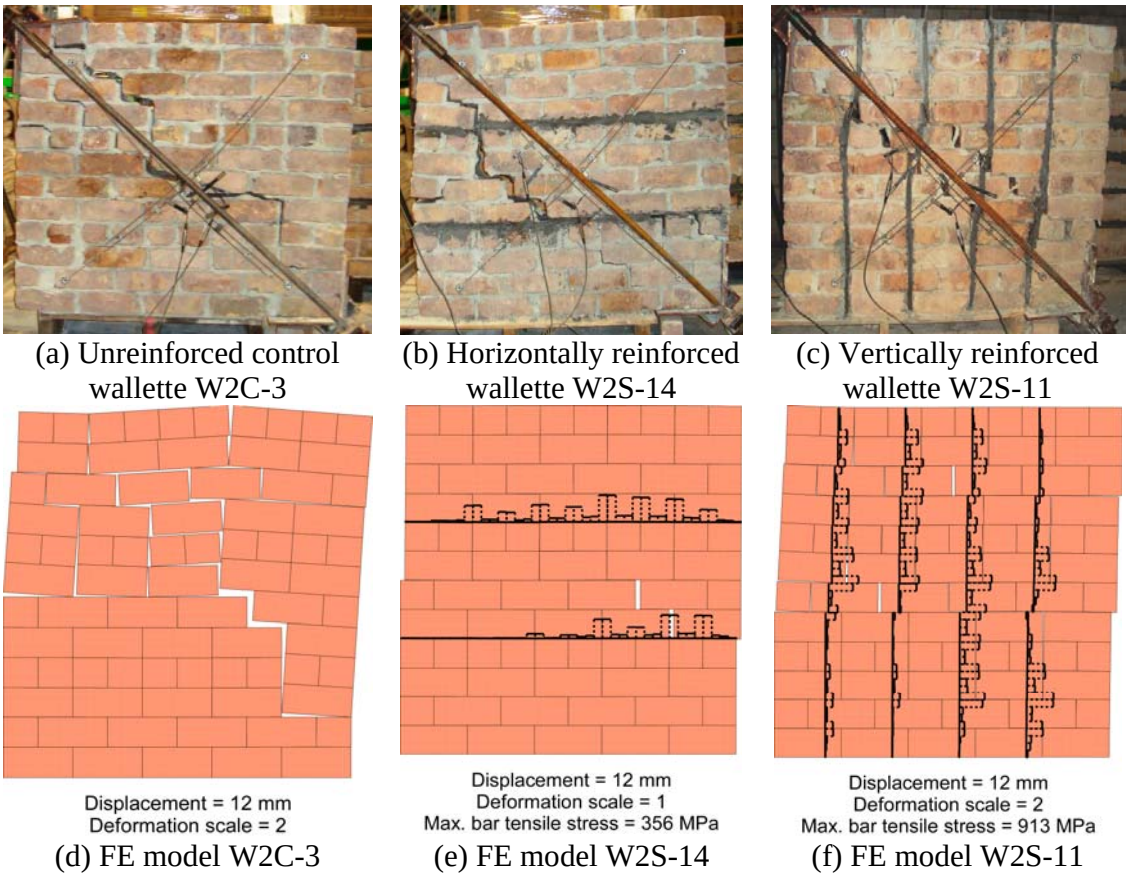

(a) Unreinforced control wallette W2C-3 (b) Horizontally reinforced wallette W2S-14 (c) Vertically reinforced wallette W2S-11

(d) FE model W2C-3 (e) FE model W2S-14 (f) FE model W2S-11

Figure 10. Series 2 wallette crack patterns
(FE model picture flipped horizontally to match orientation of wallettes in the photographs)